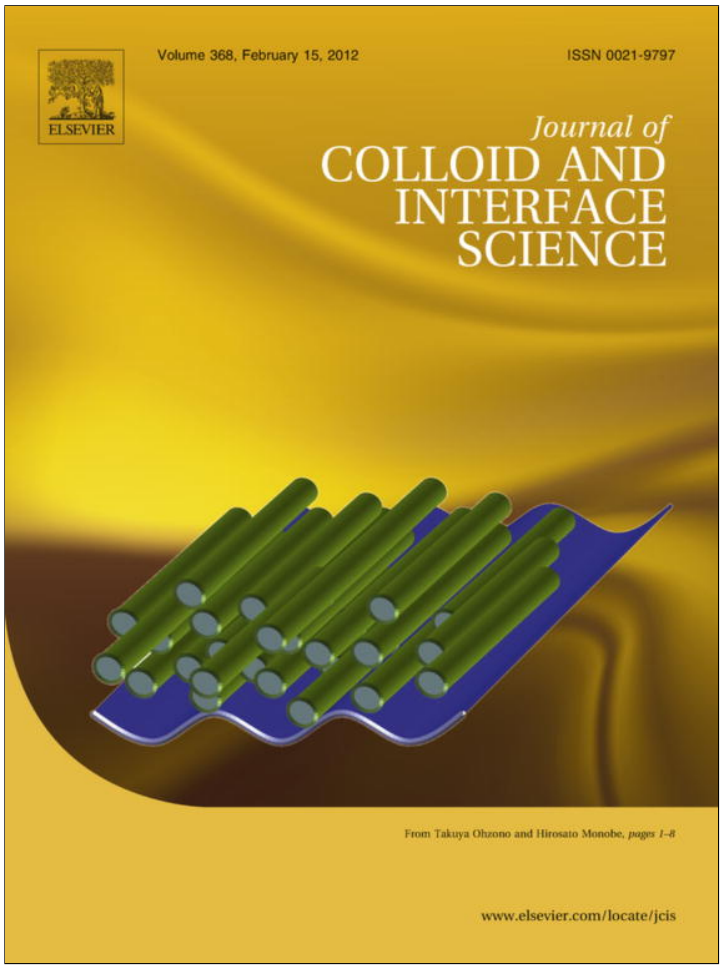

Journal of Colloid and Interface Science 368 (2012) 447–455

Contents lists available at SciVerse ScienceDirect

Journal of Colloid and Interface Science

www.elsevier.com/locate/jcis

Short range order at the amorphous TiO_2–water interface probed by silicic acid adsorption and interfacial oligomerization: An ATR-IR and ^{29}Si MAS-NMR study

Peter J. Swedlund [a,*], Yantao Song [a], Zoran D. Zujovic [a], Michél K. Nieuwoudt [a], Andreas Hermann [b], Grant J. McIntosh [a]

[a] Department of Chemistry, University of Auckland, Private Bag 92019, Auckland, New Zealand
[b] MacDiarmid Institute, PO Box 600, Wellington, New Zealand

ARTICLE INFO

Article history:
Received 4 August 2011
Accepted 29 October 2011
Available online 10 November 2011

Keywords:
Titanium dioxide
Silicic acid
Adsorption
Polymerization
Attenuated Total Reflectance Infrared
^{29}Si solid state NMR

ABSTRACT

Adsorption and oligomerization of H_4SiO_4 at the amorphous TiO_2–aqueous interface were studied using *in situ* Attenuated Total Reflectance Infrared (ATR-IR) and *ex situ* solid state ^{29}Si nuclear magnetic resonance (NMR). The ATR-IR spectra indicate that a monomeric silicate species is present at low silicate surface concentration (Γ_{Si}). Above a threshold Γ_{Si} linear silicate oligomers are formed and these oligomers dominate the surface at high Γ_{Si}. Interestingly the ATR-IR spectra of H_4SiO_4 on the TiO_2 surface are very similar to those previously observed on the poorly ordered iron oxide phase ferrihydrite. The ^{29}Si NMR spectrum of silicate on the TiO_2 surface shows the presence of Si in three states with chemical shifts corresponding to isolated monomers (Q_0), the ends of linear oligomers (Q_1) and the middle of linear oligomers (Q_2). The ratio of the area of the Q_1 and Q_2 peaks was ≈2:1 which is consistent with the proposed formation of linear silicate trimers by insertion of a solution H_4SiO_4 between adjacent suitably orientated adsorbed silicate monomers. A structural interpretation indicates that the observed interfacial silicate oligomerization behavior is a general phenomenon whereby bidentate silicate monomers on oxide surfaces are disposed towards forming linear oligomers by condensation reactions involving their two terminal Si–OH groups. The high surface curvature of nanometer sized spheres inhibits the formation of interfacial silicates with a higher degree of polymerization.

1. Introduction

Titanium dioxides are wide band-gap semiconductors with applications to photocatalysis, photovoltaics, sensors and pigments [1–3]. The electronic and optical properties of TiO_2 have a complex dependence on the bulk and surface properties of the material [2,4], and the association of silicon oxides with TiO_2 can dramatically alter these properties. For example the catalytically active TiO_2 phase anatase converts to rutile at ≈700 °C, which constrains the utility of anatase. However, in mixed TiO_2/SiO_2 oxides the temperature of the anatase to rutile phase transition increases from ≈700 to 1000 °C as the amount of Si increases from 0 to 5 atom percent [5]. Studies on the chemistry and application of SiO_2–TiO_2 systems have included titanium deposited on SiO_2 [6,7], silicon deposited on TiO_2 [1,8] and sol–gel prepared mixed SiO_2–TiO_2 phases [9]. A key parameter in understanding the sol–gel prepared SiO_2–TiO_2 materials is the proportion of Ti–O–Si, Ti–O–Ti and Si–O–Si linkages. The Ti–O–Si linkages are indicative of atomic scale homogeneity while the Ti–O–Ti and Si–O–Si linkages are indicative of SiO_2 and TiO_2 phase segregation [10]. A key parameter for SiO_2 films on TiO_2 surfaces is film uniformity and this has been achieved by a two step process involving the chemisorption (herein simply termed sorption) of a siloxane onto the TiO_2 surface forming Ti–O–Si linkages, followed by thermal or photocatalytic oxidation forming Si–O–Si linkages between the monomers [1,11].

Silicon oxides can promote the catalytic activity of TiO_2 surfaces in numerous reactions [10,12] and several explanations have been proposed for this observation depending on the system under study. For example, the presence of SiO_2 modified the electronic structure of a submonolayer of TiO_2 deposited on an SiO_2 substrate [13] and this contributed to enhanced photocatalytic oxidation of chlorinated organics by mixed TiO_2–SiO_2 phases [14]. The rate of the photocatalytic oxidation of rhodamine dye by TiO_2/SiO_2 mixed oxides was increased up to 3-fold by the presence of SiO_2 groups on the oxide surface. The rate of oxidation was correlated with the amount of rhodamine sorption by the mixed oxides with both sorption and oxidation increasing to a maximum as the % SiO_2 increased from 0 to 70% [9]. The presence of silicates dramatically alters the acid–base properties of the TiO_2 surface. At low SiO_2 surface coverage adsorption experiments with pyridine have demonstrated that the TiO_2 surface drastically changes from Lewis acid

* Corresponding author. Fax: +64 9 3737 422.
E-mail address: p.swedlund@auckland.ac.nz (P.J. Swedlund).

0021-9797/$ - see front matter © 2011 Elsevier Inc. All rights reserved.
doi:10.1016/j.jcis.2011.10.073

character (electron acceptor) to Bronsted acid character (proton donor). At high SiO_2 surface coverage the surface has neither Lewis or Bronsted acid groups, consistent with the fact that the pH of zero charge of TiO_2 and SiO_2 are ≈6 and 2 respectively. At very high surface coverage TiO_2 photocatalytic activity is inhibited. For example the use of the TiO_2 phase rutile as a pigment requires it to be coated with SiO_2 to inhibit the photocatalyzed oxidation of the organic phase [1].

The current work explores the interaction between the inorganic ligand silicic acid, H_4SiO_4, and the TiO_2 surface in an aqueous suspension. There are several motivations for this study including the role of surface silicate groups in several catalytic reactions involving TiO_2 [10,12] and a comparison of H_4SiO_4 surface chemistry on titanium and iron oxides. In addition solid state ^{29}Si NMR spectra, which clearly distinguish silicates with different degrees of polymerization, can be measured for silicates on the TiO_2 surface but not for silicates on iron oxides because of the large number of unpaired electrons in the high spin Fe^{3+} ion. The interaction between silicates and TiO_2 involves sorption via Ti–O–Si bonds and the development of Si–O–Si bonds due to silicate polymerization reactions on the TiO_2 surface. Silicic acid is a weak acid with pK_A 9.8 [15] and the initial sorption reaction involves ligand exchange of surface Ti–OH groups with the H_4SiO_4. Evidence for Ti–O–Si bonding in mixed SiO_2–TiO_2 phases comes from IR and Raman [16], ^{29}Si NMR [1], and X-ray photoelectron spectroscopy (XPS) [17]. There have been no studies of the specific structure of the TiO_2 sorbed H_4SiO_4 surface complex. In the case of many other oxyanion ligands, such as phosphate [18], arsenate [19,20], formate, and acetate [21] surface complexes with a bidentate and binuclear attachment are formed on TiO_2 surfaces. This means that two oxygen ions of the ligand are coordinated to two adjacent Ti ions on the TiO_2 surface.

Infrared spectroscopy is particularly useful for the *in situ* study of silicate sorption and polymerization reactions on the TiO_2 surface because the shape of the Si–O stretching modes (ν(Si–O)) for the sorbed silicate provides insight on the symmetry of the surface complex [22] while the position of the Si–O stretching modes provides insight on the degree of silicate polymerization [23,24]. Water is a very strong absorber of IR radiation and the applicability of IR to the study of the metal oxide–water interface has been dramatically improved by the advent on Attenuated Total Reflectance IR (ATR-IR) which provides a sampling method with the required short path length. In this study we have used an amorphous TiO_2 which is an important precursor in the formation of anatase and because it has a large surface area which provides for high concentrations of adsorbed species and ATR-IR spectra with high signal to noise ratios.

Numerous studies have shown that ^{29}Si NMR is a powerful technique to discriminate between Si atoms with different degrees of polymerization in both solution [15,25] and solid phases [26,27]. Silicon in an SiO_4 unit is designated as Q^n where n is the number of Si–O–Si linkages and the ^{29}Si chemical shift becomes increasingly negative with respect to $(CH_3)_4Si$ as n increases. In the case of silicate minerals typical ^{29}Si shifts are -70 ± 4 ppm for isolated SiO_4 tetrahedra (Q^0), $\approx -80 \pm 3$ ppm for Q^1 such as in $Si_2O_7^{6-}$ dimers or the ends of linear chains, $\approx -87 \pm 1$ ppm for Q^2 such as in single silicate chains, $\approx -98 \pm 1$ ppm for Q^3 such as in silicate sheets and lastly $\approx -109 \pm 2$ ppm for Q^4 as in three dimensional silicates like quartz [28]. There is little overlap in the ranges of ^{29}Si peak positions for different degrees of polymerization. For mixed TiO_2–SiO_2 phases the high charge density of Ti means that the ^{29}Si NMR peaks are at lower ppm such as -84 ppm for Q^1, -92 to -96 ppm for Q^2 and -100 to -102 for Q^3 [26].

The study of H_4SiO_4 chemistry on the TiO_2 surface follows several papers of H_4SiO_4 chemistry on the surface of the poorly ordered iron oxide ferrihydrite [29–33]. Ferrihydrite formed by the rapid hydrolysis of ferric nitrate solutions has a primary particle size of 2–3 nm and only two broad peaks in the powder X-ray diffraction (XRD) pattern [34]. At low Si surface concentrations monomeric silicate was the only adsorbed species present on the ferrihydrite surface [31]. The ν(Si–O) region of the ATR-IR spectrum of this species indicated the formation of a silicate surface complex with a bidentate and binuclear linkage and was consistent with Fe K edge Extended X-ray Absorption Fine Structure (EXAFS) spectra of silicate complexes with iron oxides [30,31,35]. Changes in the ν(Si–O) region of the ATR-IR spectra at higher Si surface concentration indicated the formation of Si–O–Si linkages via silicate condensation reactions on the ferrihydrite surface. This condensation produced a specific oligomer that was considered to be a linear oligomeric silicate species formed by a solution H_4SiO_4 bridging two adjacent adsorbed monomeric silicates was proposed based on the ATR-IR spectra and the structure of the 021 face that has been proposed to be present on the ferrihydrite surface [31]. The formation of a particular condensed oligomeric species on the ferrihydrite was contrasted with H_4SiO_4 condensation in solution which occurs in a disordered manner and produces numerous and diverse products [36]. For this reason it was suggested that the combination of the spatial arrangement of adsorption sites at the iron oxide/water interface and the bidentate, binuclear adsorbed monomer structure were promoting a specific lateral condensation reaction between adsorbed species. The current paper uses ATR-IR and ^{29}Si solid state NMR to examine the interaction of H_4SiO_4 on amorphous TiO_2 at pH 9 as a function of Si surface concentration. A pH of 9 was used because H_4SiO_4 adsorption on $TiO_{2(am)}$ is at a maximum at this pH. The pK_{A1} of H_4SiO_4 is 9.84 [37] and the Point of Zero Charge (PZC) of TiO_2 lies between 5 and 6 [2] so at a pH of 9 the $H_4SiO_4 : H_3SiO_4^-$ ratio is ≈7:1 and the TiO_2 surface has a negative surface charge. Spectra are interpreted based on the recently proposed structural model for amorphous TiO_2 of Zhang et al. [4].

2. Materials and methods

2.1. Materials

All solutions were made from 18 MΩ cm resistivity deionized water that had been distilled, acidified to pH 4 and saturated with N_2. Adjustments to pH were made with 0.01 to 1 M isothermally distilled HCl or low carbonate NaOH solutions. Solutions were stored in polycarbonate containers which were kept either sealed or under a stream of N_2. A stock H_4SiO_4 solution was prepared by dissolving amorphous silica (1 g) in 50:50 (w/w) NaOH:H_2O (8 g) followed by dilution to 1 L. The solution was further diluted to 1.66 mM, the pH lowered to ≈8 for 1–2 days (to allow for depolymerization which is slow at pH 4) and then the pH was lowered to pH 4 and the solution saturated with N_2 to produce a stable stock solution of 1.66 mM monomeric silicic acid in 0.01 M NaCl. The rate of color development in the molybdenum yellow method [38] was used to determine that monomeric silicic acid was the only species present within the limits of detection. For the ^{29}Si NMR spectra the H_4SiO_4 solution was prepared in the same way but starting with an enriched SiO_2 with 99% ^{29}Si purchased from Cambridge Isotope Laboratories. Amorphous TiO_2 was prepared in two methods. An oxide termed $TiO_{2(a)}$ was precipitated by alkaline hydrolysis of a solution of Ti^{IV} dissolved in concentrated H_2SO_4 which was achieved by the drop wise addition of the Ti^{IV} in H_2SO_4 to water that was maintained at pH 11 ± 1 by simultaneous drop wise addition of a 50:50 NaOH:H_2O solution while the reaction vessel was stirred rapidly in a water bath at 0 °C. An oxide termed $TiO_{2(b)}$ was precipitated by the hydrolysis of titanium ethoxide in water at 0 °C using the method of Zhang et al. [4]. This involves quickly adding 29 mL water containing four drops of acetic acid to a mixture of 21 mL titanium ethoxide and 25 mL ethanol under

stirring. Based on X-ray absorption spectra (XAS) and wide angle X-ray scattering (WAXS) this $TiO_{2(b)}$ phase was described by Zhang et al. [4] as being composed of highly distorted 2 nm diameter particles with a strained "anatase-like core". In both cases the TiO_2 formed instantaneously as a white suspension and was rinsed five times with 0.1 M NaCl at pH 11 by centrifugation and decanting and was then resuspended in water. The particle size of both TiO_2 materials was too small to be discernable by transmission electron microscopy indicating particles smaller than ≈3 nm as observed by Zhang et al. [4]. The H_4SiO_4 adsorption isotherms and the ATR-IR spectra of H_4SiO_4 adsorbed on both materials were indistinguishable. Despite this the TiO_2 material has been specified as (a) or (b) for completeness. The Ti content of the suspensions was determined using the H_2O_2 colorimetric assay after dissolution of the suspension in conc. H_2SO_4 with 16 g L^{-1} $(NH_4)_2SO_4$. Powder X-ray diffraction spectra were measured on a Phillips PW 1140 goniometer using a Cu Kα source with a 0.02° 2θ step size and 2 s count time.

2.2. Adsorption experiments

For ATR-IR experiments 50 μL of a 1 g L^{-1} $TiO_{2(a)}$ suspension was deposited onto a single bounce 45° diamond ATR crystal and the water evaporated under a gentle stream of N_2. The diamond ATR crystal was placed in a flow cell and the TiO_2 film rinsed for 1 h with 0.1 M NaCl at pH 11 to remove adsorbed carbonate and then equilibrated with 0.1 M NaCl at pH 9 for between 2 and 12 h. After this time ATR-IR spectra were collected (Section 2.3) and when a stable background was obtained the solution flow was stopped, silicic acid stock solution was added to the electrolyte, the pH readjusted to 9.0, and this solution was circulated through the cell at ≈1 mL min^{-1} for the duration of the experiment. Infrared spectra were collected (with the fluid flowing) over time for up to 48 h after which time there was little change in the collected spectra as a function of time. The solution H_4SiO_4 concentration did not change appreciably during the course of an experiment because the amount of TiO_2 present (0.5 μmol) was small compared to the amount of H_4SiO_4 in solution (50–700 μmol).

An H_4SiO_4 adsorption isotherm from 0.1 M NaCl at pH 9 was measured by equilibrating TiO_2 suspensions with a known total concentration of H_4SiO_4 (Si_T), on an end-over-end mixer for 48 h. After this time the suspensions were centrifuged and the clear supernatant filtered through a 0.2 μm membrane and the concentration of Si in solution, (Si_{sol}), measured by the molybdenum Blue method. The adsorbed Si (Si_{ads}) was determined from the difference between Si_T and Si_{sol}. All Si surface concentrations (Γ_{Si}) are given as moles of Si_{ads} per mole of Ti.

2.3. Infrared spectroscopy

A Nicolet® 8700 Spectrometer with DTGS detector and Omnic® software was used to obtain ATR-IR spectra (resolution of 4 cm^{-1}) between 4000 and 500 cm^{-1}. The spectra were corrected for changes to the water signal that affected the low wavelength side of the region of interest (between 1250 and 700 cm^{-1}) by adding or subtracting water spectra and then taking a horizontal baseline. Spectra were ATR corrected using the Omnic® advanced ATR correction algorithm. Negative Savitsky–Golay 2nd derivatives were calculated to assist band identification using an order of three and with the number of points depending on the signal to noise ratio in the original spectra. The matrix of IR spectra contained 49 rows and 261 columns representing 49 measured spectra between ≈1250 and 750 cm^{-1}. This matrix was analyzed by Principle Component Analysis (PCA) and then Multivariate Curve Resolution with Alternating Least Squares (MCR-ALS) in Matlab (Mathworks®) using the constraints of non-negative concentration and non-negative spectra [39]. MCR-ALS analysis was used to decompose the data matrix (termed "**D**") into the product of two matrices; the spectra matrix (termed "**S**") with x rows and 261 columns, representing the spectra of each of the x pure surface species and the composition matrix (termed "**C**") with 49 rows and x columns representing the contribution of each of the x surface species to each measured spectrum. MCR-ALS was used to optimize **C** and selected rows from **S** to minimize the difference between the **D** and the product **CS.** This is illustrated below for $x = 3$.

$$\mathbf{D} = \begin{bmatrix} d_{1,1} & d_{1,2} & \cdots & d_{1,261} \\ d_{2,1} & & & \vdots \\ \vdots & \ddots & & \vdots \\ \vdots & & \ddots & \vdots \\ d_{49,1} & \cdots & \cdots & d_{49,261} \end{bmatrix}$$

$$\mathbf{C} = \begin{bmatrix} c_{1,1} & c_{1,2} & c_{1,3} \\ c_{2,1} & \vdots & \vdots \\ \vdots & \vdots & \vdots \\ \vdots & \vdots & \vdots \\ c_{49,1} & c_{49,2} & c_{49,3} \end{bmatrix} \quad \mathbf{S} = \begin{bmatrix} S_{1,1} & S_{1,2} & \cdots & S_{1,261} \\ S_{2,1} & \cdots & \cdots & S_{2,261} \\ S_{3,1} & \cdots & \cdots & S_{3,261} \end{bmatrix}$$

$$d_{m,n} \cong c_{m,1} \times s_{1,n} + c_{m,2} \times s_{2,n} + c_{m,3} \times s_{3,n}$$

2.4. Solid state ^{29}Si NMR

Solid-state NMR spectra were measured on a freeze dried $TiO_{2(b)}$ sample with ^{29}Si enriched H_4SiO_4 using a Bruker AVANCE 300 spectrometer operating at 300.13 MHz proton and 59.63 MHz ^{29}Si frequency. The ^{29}Si spectrum was obtained using the standard one-pulse-and-collect sequence (Bloch decay) with heteronuclear decoupling during the acquisition interval. The spectral width was 20 kHz. The sample was spun using a 7 mm Bruker double tuned probe with zirconia rotors. The recycle delay was determined from the experiments with recycle delay increased from 50 up to 300 s until the relative peak intensities remained unchanged. The recycle delay for the final experiment was 150 s and the spectrum was obtained using 450 scans. Rotation speed was 7 kHz. Line broadening of 60 Hz was applied before Fourier transform.

3. Results and discussion

3.1. Macroscopic properties

The XRD patterns of freeze dried TiO_2 prepared by both methods are shown in Fig. 1. The main feature was a broad, low

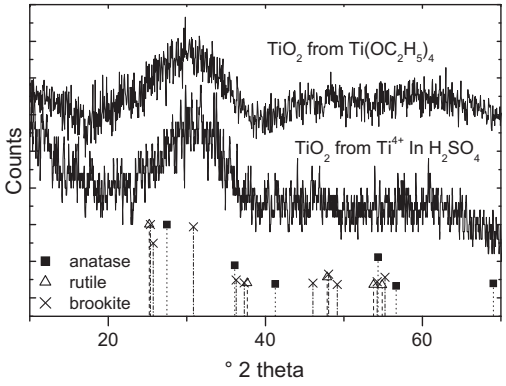

Fig. 1. The XRD pattern (Cu Kα) of the freeze dried TiO_2 samples shown with peak positions for the standard TiO_2 crystalline phases.

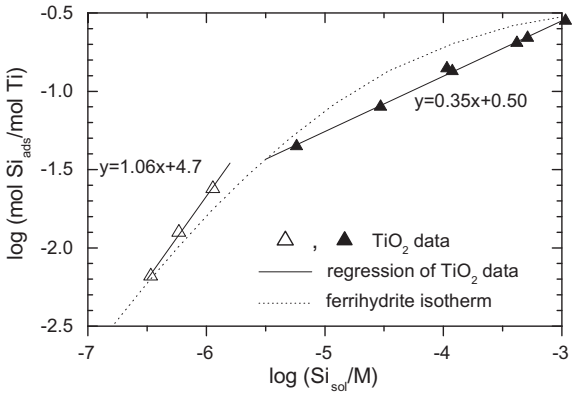

Fig. 2. The H_4SiO_4 adsorption isotherm on a $TiO_{2(am)}$ suspension at pH 9 from 0.1 M NaCl shown with the isotherm for H_4SiO_4 on ferrihydrite modeled for the same conditions using the parameters from Swedlund et al. [32].

intensity peak which coincides with one of the main brookite lines as was observed by Zhang et al. [4] for TiO_2 prepared by titanium ethoxide hydrolysis. The similarity in the XRD patterns between the two TiO_2 oxides is consistent with the similarity in the H_4SiO_4 adsorption isotherms and the ATR-IR spectra of adsorbed H_4SiO_4 on both materials and the structural model for amorphous TiO_2 developed by Zhang et al. [4] was used to interpret the H_4SiO_4 surface chemistry in the current study.

The isotherm for H_4SiO_4 adsorption onto a $TiO_{2(a)}$ suspension at pH 9 has two distinct regions (Fig. 2). At $\Gamma_{Si} < 10^{-1.4}$ the log–log isotherm had a slope of unity while the region of the isotherm with $10^{-1.4} < \Gamma_{Si} < 10^{-0.5}$ had a slope of 0.30 over two orders of magnitude in Si_{sol}. This implies that adsorption at $\Gamma_{Si} < 10^{-1.4}$ involves a single type of reaction occurring at adsorption sites that are energetically equivalent (i.e. Langmuir adsorption) but at $\Gamma_{Si} > 10^{-1.4}$ more complex surface processes are evident such as site heterogeneity or chemical interactions between adsorbing species. The ATR-IR data discussed in Section 3.2 show that chemical interactions between the sorbed monomers occurs at $\Gamma_{Si} > 10^{-1.4}$ and this can account for the change in isotherm slope [32]. Experimental data for ferrihydrite under the same conditions is not available but the isotherm modeled for the same conditions using the parameters from Swedlund et al. [32] (shown in Fig. 2) is surprisingly similar in shape and position to the isotherm measured for TiO_2.

3.2. ATR-IR spectra of H_4SiO_4 adsorbed on am-TiO_2

3.2.1. General trends

The ν(Si–O) region of IR spectra measured over time as films of $TiO_{2(a)}$ were exposed to Si_{sol} between 0.097 and 1.34 mM are shown in Fig. 3. Many aspects of the ATR-IR spectra of H_4SiO_4 on TiO_2 were very similar to those observed for H_4SiO_4 on ferrihydrite [32] and the spectra are discussed only briefly. The area of the ν(Si–O) feature in the IR spectra (termed $A_{\nu(Si-O)}$) increased approximately linearly as a function of the log of time at each Si_{sol} (Fig. 4a). This type of adsorption kinetics has been observed for several systems in which small molecules are adsorbing onto metal oxides and has been attributed to either site heterogeneity and interparticle or intraparticle diffusion [40]. For TiO_2 films exposed to Si_{sol} of either 0.097 or 1.34 mM the maximum IR absorbances after ≈30 h were 0.006 and 0.054 respectively. This can be compared to the maximum IR absorbance of 0.00016 for a 1.66 mM H_4SiO_4 solution under the same ATR conditions but without the TiO_2 film deposited on the ATR crystal [30,41]. A solution with 1.66 mM H_4SiO_4 is 10% below the solubility product of an amorphous SiO_2 precipitate [15] which demonstrates that the H_4SiO_4 contained in the volume of the TiO_2 film that is sampled by the ATR-IR beam is up to 300 times more concentrated than a saturated H_4SiO_4 solution. Precipitation of SiO_2 is not observed because the H_4SiO_4 is adsorbed on the oxide surface. It is also evident that the solution H_4SiO_4 does not contribute appreciably to the measured spectra of adsorbed H_4SiO_4.

In all cases the spectra collected immediately after introduction of H_4SiO_4 had a maximum IR absorbance at ≈960 cm^{-1}. At the

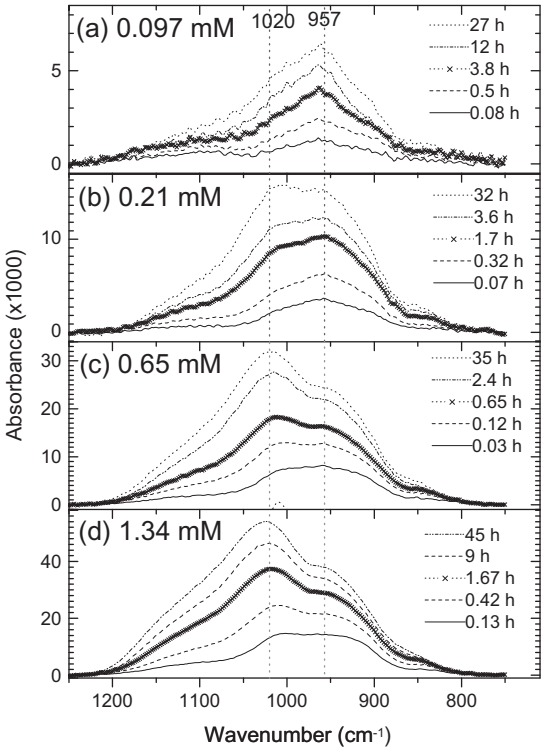

Fig. 3. ATR-IR spectra of H_4SiO_4 adsorbed on amorphous TiO_2 at pH 9 and 0.1 M NaCl measured over time. Final concentrations of H_4SiO_4 are shown in the figure.

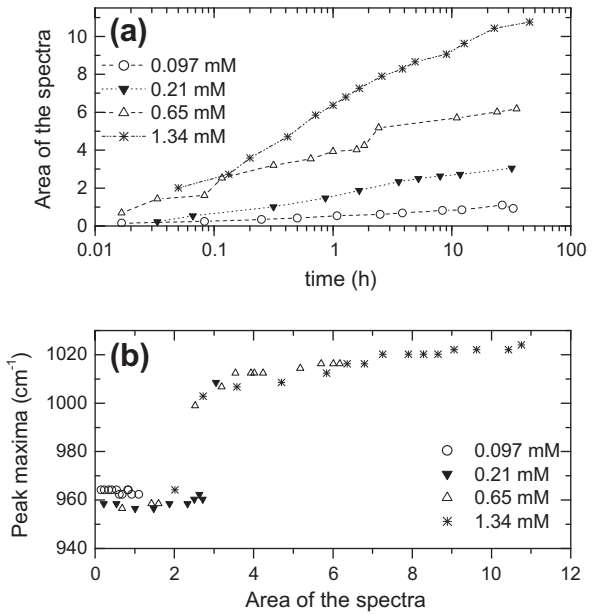

Fig. 4. Properties of the Si–O stretching region in the ATR-IR spectra measured over time as H_4SiO_4 adsorbed on amorphous TiO_2 at pH 9 and 0.1 M NaCl. (a) The area of the spectra and (b) the position of the maximum IR absorbance. Final solution Si concentrations are shown in the figure legends.

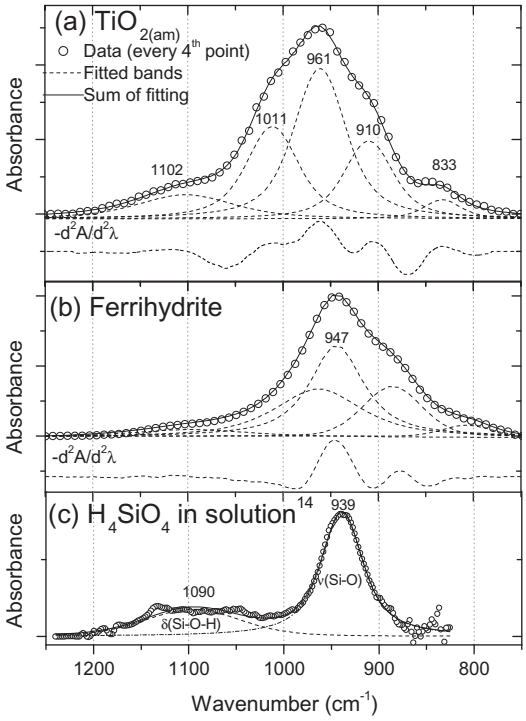

Fig. 5. The ATR-IR spectra and band fitting of (a) the low Γ_{Si} species on amorphous TiO_2 (b) the low Γ_{Si} species on ferrihydrite [30] (c) H_4SiO_4 in solution [41].

lowest Si_{sol} of 0.097 mM the shape of the spectra did not change over the 27 h of the experiment. For each experiment with Si_{sol} > 0.097 mM the IR absorption in the region of ≈1015 cm^{-1} increased as Γ_{Si} increased over time and this feature became more prominent at higher H_4SiO_4 concentration. For example with 0.21 mM H_4SiO_4 the feature at ≈1015 cm^{-1} developed over time to become the dominant spectral feature after 32 h while with 0.65 mM H_4SiO_4 the spectral feature at 1015 cm^{-1} dominated the spectra after 0.12 h. Examining the absorbance scales in Fig. 3 it is evident that at each Si_{sol} the IR absorbance at ≈1015 cm^{-1} exceeded the IR absorbance at ≈960 cm^{-1} only when the maximum IR absorbance was >0.01. Similarly the wavenumber of maximum IR absorbance increased from ≈960 to 1015 cm^{-1} when the area of the Si–O stretching feature exceeded ≈2.6 (Fig. 4b). This implies that there is some threshold H_4SiO_4 surface concentration on the $TiO_{2(am)}$ where the silicate species that absorbs at 1015 cm^{-1} becomes the dominant surface species.

3.2.2. Spectra at low Γ_{Si}

When $A_{\nu(Si-O)}$ was <1 the IR spectra had the same shape and the average of these spectra is shown in Fig. 5a. The maximum IR absorbance occurred at 960 cm^{-1} and this band had shoulders on either side of it which are particularly evident in the 2nd derivatives. In addition there is a smaller shoulder at 830 cm^{-1} and a broad band at around 1100 cm^{-1}. The position and shape of this spectral feature provides insights into the structure of the adsorbed silicate under these conditions. The IR spectrum of H_4SiO_4 in solution (Fig. 5c) has an asymmetric triply degenerate ν(Si–O) mode at 939 cm^{-1} and a broad weak Si–O–H bending mode at ≈1090 cm^{-1} while the symmetric Si–O stretch occurs at 787 cm^{-1} in the Raman spectrum [41]. The spectra of H_4SiO_4 adsorbed on TiO_2 at low Γ_{Si} are similar, but at slightly higher frequency, to those of for the monomeric adsorbed H_4SiO_4 on ferrihydrite at low Γ_{Si} (Fig. 5b) [30]. The spectra of the monomeric silicate on the ferrihydrite surface did not change with pH between 4 and 10, or with ionic strength between 0.01 and 0.1 M [32,33].

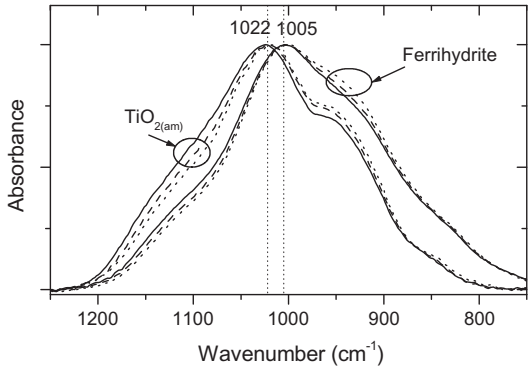

Fig. 6. Several ATR-IR spectra of H_4SiO_4 adsorbed at high surface coverage on amorphous TiO_2 (this study) or ferrihydrite (Swedlund et al. [30]). All spectra are scaled to the maximum absorbance. For each oxide the surface coverage decreases in the order solid > dashed > dotted lines.

The three asymmetric ν(Si–O) bands are all clearly resolved in the silicate on TiO_2 spectrum compared to the spectrum for ferrihydrite where two ν(Si–O) bands at ≈946 cm^{-1} were not resolved [30]. Both the higher frequency and greater splitting of the ν(Si–O) bands for H_4SiO_4 adsorbed on TiO_2 are consistent with the higher charge density of the Ti^{4+} cation compared to that of Fe^{3+}. The spectra indicate that H_4SiO_4 adsorbed on TiO_2 at low Γ_{Si} is present as a monomeric silicate surface complex with asymmetric ν(Si–O) bands at 910, 961 and 1011 cm^{-1}, the symmetric ν(Si–O) band is weakly IR active at 833 cm^{-1} while the broad band at ≈1100 cm^{-1} is the Si–O–H bending mode. The IR spectra indicate a bidentate surface similar to the monomeric H_4SiO_4 surface complex on the iron oxide surface [30,35].

3.2.3. ATR-IR spectra at high Γ_{Si}

As the $A_{\nu(Si-O)}$ increased from ≈1 to 5 the shape of the spectra changes from having a maximum absorbance at ≈960 cm^{-1} to a spectrum with a maximum at ≈1020 cm^{-1}. However, as $A_{\nu(Si-O)}$ increases from ≈5 to 10 the ATR-IR spectra have a similar shape (Fig. 6), apart from a small decrease in the IR absorbance around 950 cm^{-1} and a small increase in IR absorbance around 1100 cm^{-1}. At these high Γ_{Si} the IR spectra of H_4SiO_4 adsorbed on the $TiO_{2(am)}$ have the same shape as those observed at high Γ_{Si} on ferrihydrite [31] but, as observed at low Γ_{Si}, they are at slightly higher frequency. This implies the same linear oligomers are formed on the surfaces of both oxides. The structural interpretation for the TiO_2 surface is presented in Section 3.3.

The last feature in the ATR-IR spectra is the small increase in IR absorbance intensity between 1050 and 1150 cm^{-1} observed at high Γ_{Si} in Fig. 6 and this feature can be attributed to the development of an $SiO_{2(am)}$ on the $TiO_{2(am)}$ surface [30]. This high Γ_{Si} feature made a comparatively small contribution to the measured IR spectra for the $TiO_{2(am)}$ system even when $Si_{(sol)}$ was just 30% below saturation with respect to precipitation of a bulk $SiO_{2(am)}$ phase. This indicates that the $TiO_{2(am)}$ surface promotes the formation of an oligomeric silicate phase but does not strongly promote the formation of three dimensional polymers.

3.2.4. Quantitative analysis of the ATR-IR spectra

The matrix of all 49 measured spectra (each with 261 data points) were analyzed by MCR-ALS. Prior exploratory analysis of the data using PCA gave eigenvalues similar to the values reported for the ferrihydrite data [31] and were consistent with the proposed model of two main surface species and a third minor species. In the MCR-ALS analysis the monomer spectrum was fixed to the average of the spectra at low Γ_{Si} (Fig. 5a), the oligomer spectrum

was optimized with the initial estimate being the average of the high Γ_{Si} spectra (Fig. 6), and the polymer spectrum was optimized from an initial estimate from the data for ferrihydrite [31]. The optimized model fitted the details of the measured ATR-IR spectra very closely and the largest residual for any spectrum was on average 2% of the largest IR absorbance of that spectrum. The optimized pure spectra for the surface species and typical fits to measured spectra using these spectra are shown for various surface compositions in Fig. SI 1.

The contributions that each surface species made to the area of the measured spectra as H_4SiO_4 adsorbs onto $TiO_{2(am)}$ over time were similar to that observed on ferrihydrite and are shown in Fig. SI 2. At each $Si_{(sol)}$ the monomeric species adsorbs initially and then the oligomer species starts to form after some lag period. The lag phase before oligomer formation is shorter at higher $Si_{(sol)}$. For example, the lag phase decreased from ≈10 to 0.1 h as $Si_{(sol)}$ increased from 0.097 to 0.65 mM. At each $Si_{(sol)}$ the growth of oligomer was delayed until a certain surface coverage of monomer was obtained corresponding to a component spectral area of ≈1. The contributions that each surface species made to the area of the measured spectra as H_4SiO_4 adsorbs onto $TiO_{2(am)}$ are shown as a function of $A_{\nu(Si-O)}$ in Fig. 7. The data for all $Si_{(sol)}$ from 0.097 to 1.34 mM follow the same trend indicating that the distribution of surface species at a given surface concentration is independent of solution concentration. The quantitative analysis agrees with the qualitative analysis in that as Γ_{Si} increased the surface changes from being predominantly monomeric when $A_{\nu(Si-O)} < 2$ to being predominantly oligomeric at $A_{\nu(Si-O)} > 5$.

3.3. ^{29}Si solid state NMR of H_4SiO_4 adsorbed on amorphous TiO_2

Approximately 0.3 g of sample was needed for the NMR analysis and this was obtained by equilibrating a suspension of $TiO_{2(b)}$ (0.06 g L^{-1}) with 99% ^{29}Si enriched H_4SiO_4 (0.28 mM total concentration) at pH 9 in 0.1 M NaCl. Preliminary experiments with TiO_2 suspensions were undertaken with natural abundance H_4SiO_4 (i.e. 5% ^{29}Si) where the equilibrated TiO_2 pastes were collected by centrifugation and ATR-IR spectra measured against TiO_2 pastes with no Si. This was done to choose appropriate TiO_2 and H_4SiO_4 concentrations that would result in a sample with appreciable amounts of both monomeric and oligomeric adsorbed H_4SiO_4 for the ^{29}Si NMR analysis. In addition the sample for NMR analysis was freeze dried and ATR-IR spectra were measured on the freeze-dried powder to compare with the spectrum from the undried paste to assess for changes during drying. The ATR-IR spectra

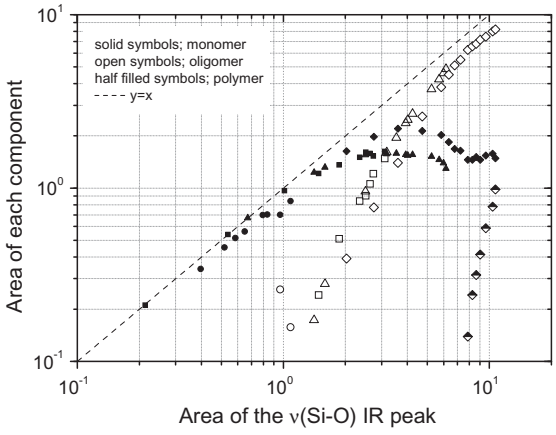

Fig. 7. Surface speciation as a function of surface concentration for H_4SiO_4 adsorbing over time onto amorphous TiO_2 from 0.1 M NaCl at pH 9. The solution Si was 0.097 mM (circles), 0.21 mM (squares), 0.65 mM (triangles) and 1.34 mM (diamonds).

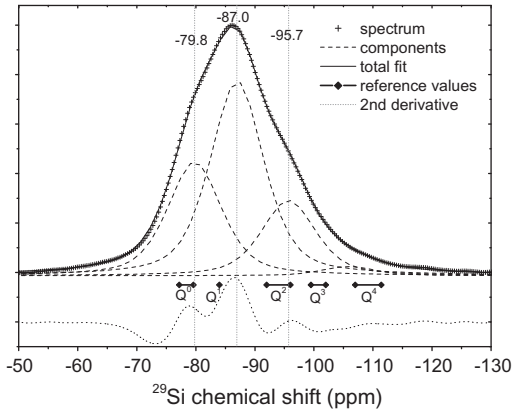

Fig. 8. The ^{29}Si solid state NMR spectrum of $H_4{}^{29}SiO_4$ on $TiO_{2(b)}$ with $\Gamma_{Si} = 0.18$. Reference values are for mineralogical samples and TiO_2–SiO_2 mixed phases as detailed in the text [8,26,42].

of the $H_4{}^{29}SiO_4$ on the TiO_2 paste and the TiO_2 after freeze drying (Fig. SI 3) were very similar with slightly less IR absorbance in the dried sample around 940 cm^{-1} indicating a small amount of silicate condensation upon drying. The MCR-ALS fitting indicated that the monomeric component comprised 50 and 55% of the area of the ATR-IR spectra for the dried sample and paste sample respectively.

The main peak in the NMR spectrum of this sample (Fig. 8) occurs at ≈−87 ppm and there are clearly shoulders on either side of this peak, at −79.8 and −95.7 ppm. In addition there is a tail extending on the more negative side of the peak at ≈−105 ppm. The ^{29}Si NMR peak position for a Q^n Si depends primarily on the value of n but for Si with the same Q^n the peak position become more negative for higher charge densities of the cations to which the silicates are coordinated [42,43]. Therefore to assign the peaks in the spectrum it is necessary to refer to materials where silicates are coordinated with Ti^{4+} cations. The peak at −79.8 ppm is within the range observed for Q^0 Si including the orthosilicate mineral titanite $CaTiSiO_5$ (−79.6 ppm) [42] and also Q^0 Si presumed to occupy interstitial sites in a rutile sample (−77.3 ppm) [42]. Similarly the peak at −95.7 ppm is within the range for Q^2 Si in sol–gel prepared mixed TiO_2–SiO_2 oxides (−92 to −96 ppm) [8,26] and in the cyclosilicate mineral benitoite (−94.2) [42]. Only one reference value for Q^1 Si was found which was for a mixed TiO_2–SiO_2 oxide (−84 ppm) [26] and it is clear that the peak at −87 ppm is Q^1. The tail at ≈−105 ppm indicates a small amount of silicate with Q^3–Q^4 but the peak is too weak to allow for definitive peak fitting.

The NMR spectrum qualitatively agrees with the proposed model for H_4SiO_4 polymerization at an oxide surface. The Q^0 peak corresponds to the monomeric adsorbed H_4SiO_4, while the Q^1 and Q^2 peaks correspond to terminal and middle Si in linear silicate oligomers. Other possible surface silicate oligomers can be excluded. For example a cyclic silicate species would have all Q^2 and a branched silicate would have Q^1–Q^3 Si present. The percentage of the NMR spectrum due to the monomeric silicate was 30% compared with 50% of the ATR-IR spectrum. The conditions of collecting the NMR spectra were chosen so that the NMR signal will be directly quantitative for the different types of silicate [26] whereas the ATR-IR signal is only approximately quantitative. The ratio of Q^1 and Q^2 peak areas would be 1:0.5 for a linear trimer whereas the measured value was 1:0.4. Longer linear oligomers would have larger Q^2 areas (e.g. 1:1 for a tetramer) and a dimeric species would have no Q^2 peak [25]. In addition the *in situ* ATR-IR spectra experiments on the TiO_2 and the ferrihydrite indicate the formation of an oligomer which is predominantly one species which is larger than a dimer and which forms directly from the monomeric silicates. Possible explanations for the slightly higher

measured Q^1:Q^2 include a small proportion of either a dimeric silicate or a branched tetramer with Q^1:Q^3 of 1:0.3. The later option would also explain the small Q^3–Q^4 peak in the NMR spectrum.

3.4. Structural interpretation

The fact that the same silicate oligomerization product is formed on the surface of two different poorly ordered oxides suggest that this is a general phenomenon whereby bidentate silicate monomers on an oxide surface are disposed towards forming linear oligomers by condensation reactions involving their two terminal Si–OH groups. In this section we explore if the formation of short one dimensional oligomers on the TiO_2 surface is structurally reasonable based on geometric constraints of silicate polymerization and the structural model for amorphous TiO_2 developed by Zhang et al. [4] based on a combination of reverse Monte Carlo and Molecular Dynamics simulations of wide-angle X-ray scattering data and X-ray adsorption spectra. Zhang et al. [4] kindly provided the atomic coordinates for their structural model of TiO_2 particles containing 123 Ti atoms, 246 O atoms and having an irregular "potato" shape as shown in Fig. SI 4. The particles had a diameter of ≈2 nm with a small strained "anatase-like" core and a highly distorted shell [4]. The $TiO_{2(am)}$ structural model therefore represents a disordered surface and the applicability of this interpretation of silicate oligomerization to other disordered surfaces, such as ferrihydrite, will be considered.

The average Ti coordination number was 5.3 due to the truncation of the many TiO_6 octahedra on the particle surface. In an aqueous suspension H_2O will complete the coordination sphere of the coordinatively unsaturated surface Ti ions such that, after deprotonation, the surface will have a large number of terminal Ti–OH groups. For an irregular oxide particle there is no rigorous process for defining which Ti ions are on the surface. For this work Ti ions which were clearly beneath other Ti ions were excluded leaving 88 Ti atoms. The average coordination numbers of the outer 88 Ti ions and the inner 35 Ti ions were 5.05 and 6.00 respectively. There were 67 of the 88 outer Ti ions that had a coordination number less than six and these Ti ions were considered to be surface active.

Geometric constraints for surface monomer and oligomer adsorption sites are proposed based on the range of Si–O bond distances and angles observed in silicate minerals. Liebau [44] reports that Si–O distances vary between 1.57 and 1.72 Å, O–Si–O angles vary between 98 and 122° while the Si–O–Si angles vary between 120 and 180°. Adjacent terminal Ti–OH groups that are sufficiently close to be bridged by a H_4SiO_4 tetrahedra will provide sites that can undergo ligand substitution producing a monomeric silicate surface complex. The average distance between nearest neighbor surface Ti atoms is 3.1 Å (σ = 0.18 Å). A slightly larger distance of 3.5 Å was taken to be a maximum Ti–Ti distance for monomer H_4SiO_4 adsorption (d in Fig. 9) based on the edges of SiO_4 tetrahedra in minerals which range from 2.4 to 3.0 Å [44] and the possibility of the surface oxygen ions being closer than the underlying Ti atoms. There are 66 surface Ti–Ti pairs at a distance less than 3.5 Å and three isolated Ti ions as shown in Fig. 10 which is explained more fully below.

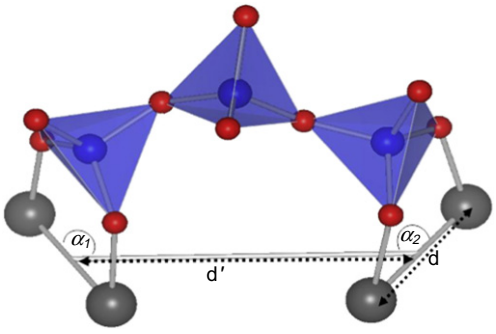

Fig. 9. A linear silicate trimer (blue tetrahedra) formed between four Ti ions (gray spheres) to illustrate the scheme for structural constraints for H_4SiO_4 oligomerization on the $TiO_{2(am)}$ surface. The extreme case where d' = 6.5 Å and $\alpha_1 = \alpha_2$ = 120° is shown. (For interpretation of the references to color in this figure legend, the reader is referred to the web version of this article.)

Sites for oligomerization require adjacent monomers with an appropriate distance and orientation for insertion of a solution H_4SiO_4. The geometric constraints for oligomers to form between adjacent monomers are based on the position of the Ti cations because of the large number of degrees of freedom to consider in the range of Si–O bond distances and angles. The geometric constraints are based on the length (d') of the line that connects the midpoints of the two Ti–Ti pairs and the angles (α_1 and α_2) between this line and the lines between each Ti–Ti pair (Fig. 9). Values of d' between 3 and 6.5 Å combined with α_1 and α_2 values between 60 and 120° (i.e. within 30° of normal) were considered reasonable for oligomerization between adjacent monomers based on empirical tests. For example Fig. 9 shows a trimer on a base with d' = 6.5 Å,

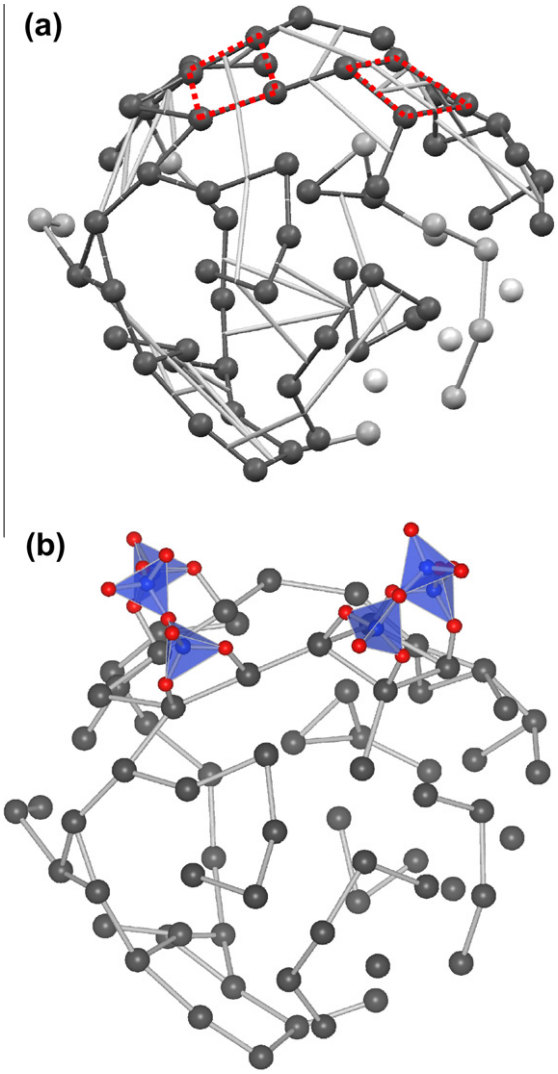

Fig. 10. The arrangement of monomer and oligomer sites on the $TiO_{2(am)}$ model of Zhang et al. [4]. (a) All spheres are Ti. Lines between spheres depict monomer sites and lines between midpoints depict oligomer sites. The Ti are from darkest to lightest the oligomerization sites, monomer sites only and isolated Ti ions. The red quadrilaterals depict the sites for the two adjacent trimers depicted in (b). (For interpretation of the references to color in this figure legend, the reader is referred to the web version of this article.)

$\alpha_1 = \alpha_2 = 120°$ and oligomer formation can occur within the range of observed Si–O bond lengths and angles in minerals at this extreme of the constraints even where the Ti–O bonds are constrained to be within 10° of normal to the surface. For values of d' close to 3 Å the fact that the minimum Ti–Ti distance is at 2.9 Å further constrains α_1 and α_2. For example when $d' = 3$ Å then α_1 and α_2 must be such that the two monomer edges of the quadrilateral are within 5° of being parallel. The dihedral angle was not specifically constrained other than its effect on α_1 and α_2. With these constraints there are 40 sites for oligomerization on a $TiO_{2(am)}$ particle surface. Of the 67 surface Ti ions 54 are part of a potential oligomerization site, 10 are part of monomer sites that are not predisposed to oligomerization while three are not part of monomer or oligomer sites. With these constraints the Si/Ti ratio at maximum surface coverage would be 0.36 compared to largest value measured from the isotherm of 0.29 (Fig. 2).

This model of the surface is depicted in Fig. 10a which shows oligomers can form on most of the particle surface. From this argument it would appear to be reasonable that oligomers can dominate the surface at high Γ_{Si}. Lastly we consider the amount of monomeric and polymeric silicate on the surface. At the highest Γ_{Si} the amount of monomeric silicate (Fig. 7) plateaus to be approximately 10% of the surface silicate rather than decreasing to zero if all monomers were replaced with oligomers. The outcome from the application of the geometric constraints implied that some monomer sites would not be predisposed to oligomerization but the constraints were deliberately conservative. In addition it is evident that as oligomers form on the surface this will preclude the formation of oligomers at other sites and some adsorbed monomers will become isolated. In addition the formation of pentamers from a monomer and an adjacent trimer will be subject to more stringent structural constraints relating to silicate groups at the end of a trimers constrained movement. Lastly we discuss the observation that the TiO_2 surface is not predisposed to the formation of three dimensional polymers. Fig. 10b shows the relationship between adjacent adsorbed trimers. It is clear that adjacent trimers are orientated away from each other because of the high curvature of the surface of the small diameter TiO_2 particle. The distance between terminal hydroxide groups on the adjacent trimers range from 8 to 12 Å which is too large to be bridged by a solution H_4SiO_4.

The similarity in the H_4SiO_4 oligomerization chemistry on the poorly ordered oxides of both Ti^{IV} and Fe^{III} suggests the proposed interpretation of silicate oligomerization may be more generally applicable to disordered surfaces, such as 2-line ferrihydrite. From simple geometric arguments nanometer sized oxide particles will have both a high curvature and also a high surface concentration of coordinatively unsaturated cations that will produce surface hydroxyl groups in water. These are the basic features of the proposed silicate oligomerization model. While various structural models for ferrihydrite have been proposed and refuted [45–48] the $TiO_{2(am)}$ model indicates that nanometer sized particles with crystalline cores will tend to have a highly strained and disordered surface because of the constraints of high surface curvature. The primary particle size of 2-line ferrihydrite is 2–3 nm [45] which is comparable to that of $TiO_{2(am)}$. In addition the proposed concentration of monomer adsorption sites are comparable on the two oxides i.e. 0.26 per Ti for $TiO_{2(am)}$ and 0.2 per Fe for ferrihydrite [32]. These structural and morphological similarities may explain the similar silicate surface chemistry on the ferrihydrite and $TiO_{2(am)}$.

4. Conclusions

Attenuated Total Reflectance IR and ^{29}Si NMR were used to study the adsorption and interfacial condensation reactions of H_4SiO_4 on the surface of an amorphous TiO_2 at pH 9. At low Si surface concentration the IR spectra show that the interfacial silicate is present as monomers with maximum IR absorption at $\approx$960 cm^{-1}. Condensed oligomeric surface species with Si–O–Si linkages and a maximum IR absorbance at $\approx$1020 cm^{-1} are formed once a threshold surface concentration of silicate monomers was reached. The condensed silicate surface species was considered to be a linear oligomer formed by a solution H_4SiO_4 bridging adjacent monomers. The data were interpreted using the atomic coordinates for a structural model of amorphous TiO_2 and the geometric constraints of silicate polymerization observed in mineral systems. The surface of the amorphous TiO_2 was conducive to the formation of linear silicate oligomers because it held adjacent monomers in a configuration which allowed for bridging by a solution H_4SiO_4. Despite the predominance of oligomeric silicate on the TiO_2 surface the formation of three dimensional polymeric silicates was minimal, even close to solution saturation with respect to a pure SiO_2 phase. This was attributed to the small diameter and high surface curvature of the TiO_2 particles which keeps adjacent oligomers at too large a distance to be bridged by solution H_4SiO_4.

Acknowledgments

The authors wish to thank Hengzhong Zhang from the University of California Berkley for kindly providing the atomic coordinates for amorphous TiO_2 and for helpful and friendly advice. Bryon Wright (University of Auckland) is thanked for help manipulating matrices. PJS, AH and YS thank the NZFRST and Mighty River Power (NZ) for funding.

Appendix A. Supplementary material

Supplementary data associated with this article can be found, in the online version, at doi:10.1016/j.jcis.2011.10.073.

References

[1] N. Mukaihata, H. Matsui, T. Kawahara, H. Fukui, H. Tada, J. Phys. Chem. C 112 (2008) 8702.
[2] X. Chen, S.S. Mao, Chem. Rev. 107 (2007) 2891.
[3] G. Pfaff, P. Reynders, Chem. Rev. 99 (1999) 1963.
[4] H.Z. Zhang, B. Chen, J.F. Banfield, G.A. Waychunas, Phys. Rev. B 78 (2008) 214106.
[5] K. Okada, N. Yamamoto, Y. Kameshima, A. Yasumori, K.J.D. MacKenzie, J. Am. Ceram. Soc. 84 (2001) 1591.
[6] J.L. Lu, K.M. Kosuda, R.P. Van Duyne, P.C. Stair, J. Phys. Chem. C 113 (2009) 12412.
[7] H.L. Tang, C.H. Yu, W. Oduoro, H.Y. He, S.C. Tsang, Langmuir 24 (2008) 1587.
[8] H. Tada, M. Akazawa, Y. Kubo, S. Ito, J. Phys. Chem. B 102 (1998) 6360.
[9] C. Anderson, A.J. Bard, J. Phys. Chem. 99 (1995) 9882.
[10] X.T. Gao, I.E. Wachs, Catal. Today 51 (1999) 233.
[11] H. Tada, Langmuir 12 (1996) 966.
[12] J. Abad, C. Gonzalez, P.L. de Andres, E. Roman, Phys. Rev. B 82 (2010).
[13] L. Soriano, G.G. Fuentes, C. Quiros, J.F. Trigo, J.M. Sanz, P.R. Bressler, A.R. Gonzalez-Elipe, Langmuir 16 (2000) 7066.
[14] D. Panayotov, J.T. Yates, Chem. Phys. Lett. 381 (2003) 154.
[15] A.R. Felmy, H. Cho, J.R. Rustad, M.J. Mason, J. Solution Chem. 30 (2001) 509.
[16] C.C. Perry, X.C. Li, D.N. Waters, Spectrochim. Acta Part A: Mol. Biomol. Spectrosc. 47 (1991) 1487.
[17] B. Gallas, A. Brunet-Bruneau, S. Fisson, G. Vuye, J. Rivory, J. Appl. Phys. 92 (2002) 1922.
[18] P.A. Connor, A.J. McQuillan, Langmuir 15 (1999) 2916.
[19] G.Z. He, G. Pan, M.Y. Zhang, Z.Y. Wu, J. Phys. Chem. C 113 (2009) 17076.
[20] G.Z. He, M.Y. Zhang, G. Pan, J. Phys. Chem. C 113 (2009) 21679.
[21] F.P. Rotzinger, J.M. Kesselman-Truttmann, S.J. Hug, V. Shklover, M. Gratzel, J. Phys. Chem. B 108 (2004) 5004.
[22] K. Nakamoto, Infrared and Raman Spectra of Inorganic and Coordination Compounds Part A: Theory and Applications in Inorganic Chemistry, fifth ed., John WIley and Sons, New York, 1997.
[23] V.C. Farmer, in: V.C. Farmer (Ed.), Infrared Spectra of Minerals, Mineralogical Society, London, 1974 (Monograph No. 4).
[24] A.N. Lazarev, Vibrational Spectra and Structure of Silicates, Consultants Bureau, New York, 1972.

[25] H. Cho, A.R. Felmy, R. Craciun, J.P. Keenum, N. Shah, D.A. Dixon, J. Am. Chem. Soc. 128 (2006) 2324.
[26] P.J. Dirken, M.E. Smith, H.J. Whitfield, J. Phys. Chem. 99 (1995) 395.
[27] K.A. Smith, R.J. Kirkpatrick, E. Oldfield, D.M. Henderson, Am. Mineral. 68 (1983) 1206.
[28] E. Lippmaa, M. Maegi, A. Samoson, G. Engelhardt, A.R. Grimmer, J. Am. Chem. Soc. 102 (1980) 4889.
[29] P.J. Swedlund, J.G. Webster, Water Res. 33 (1999) 3413.
[30] P.J. Swedlund, G.M. Miskelly, A.J. McQuillan, Geochim. Cosmochim. Acta 73 (2009) 4199–4214.
[31] P.J. Swedlund, G.M. Miskelly, A.J. McQuillan, Langmuir 26 (2010) 3394–3401.
[32] P.J. Swedlund, R.D. Hamid, G.M. Miskelly, J. Colloid Interf. Sci. 352 (2010) 149–157.
[33] R. Dol Hamid, P.J. Swedlund, Y. Song, G.M. Miskelly, Langmuir 27 (2011) 12930–12937.
[34] R.M. Cornell, U. Schwertmann, The Iron Oxides: Structure, Properties, Reactions, Occurrences and Uses, second ed., Wiley-VCH, Weinheim, 2003.
[35] G.S. Pokrovski, J. Schott, F. Garges, J.L. Hazemann, Geochim. Cosmochim. Acta 67 (2003) 3559.
[36] S. Sjoberg, J. Non-Cryst. Solids 196 (1996) 51.
[37] J.P. Gustafsson, 2006.
[38] G.B. Alexander, J. Am. Chem. Soc. 75 (1953) 5655.
[39] R. Tauler, A. Smilde, B. Kowalski, J. Chemometr. 9 (1995) 31.
[40] J. Zhang, R. Stanforth, Langmuir 21 (2005) 2895.
[41] G.J. McIntosh, P.J. Swedlund, T. Sohnel, Phys. Chem. Chem. Phys. 13 (2011) 2314.
[42] J.F. Stebbins, in: T.J. Ahrens (Ed.), Mineral Physics & Crystallography: A Handbook of Physical Constants, American Geophysical Union, Washington DC, 1995.
[43] J.F. Stebbins, MRS Bull. 17 (1992) 45.
[44] F. Liebau, Structural Chemistry of Silicates: Structure, Bonding, and Classification, Springer-Verlag, Berlin, 1985.
[45] T. Hiemstra, W.H.V. Riemsdijk, Geochim. Cosmochim. Acta 73 (2009) 4423–4436.
[46] F.M. Michel, L. Ehm, S.M. Antao, P.L. Lee, P.J. Chupas, G. Liu, D.R. Strongin, M.A.A. Schoonen, B.L. Phillips, J.B. Parise, Science 316 (2007) 1726.
[47] A. Manceau, Am. Mineral. 96 (2011) 521.
[48] A. Manceau, Clay Miner. 45 (2010) 225.